PKCβ regulates ischemia/reperfusion injury in the lung

Tomoyuki Fujita,[1] Tomohiro Asai,[1] Martin Andrassy,[1] David M. Stern,[2] David J. Pinsky,[3] Yu Shan Zou,[1] Morihito Okada,[1] Yoshifumi Naka,[1] Ann Marie Schmidt,[1] and Shi-Fang Yan[1]

[1]Department of Surgery, College of Physicians and Surgeons, Columbia University, New York, New York, USA. [2]Medical College of Georgia, Augusta, Georgia, USA. [3]Department of Medicine, College of Physicians and Surgeons, Columbia University, New York, New York, USA.

Activation of PKCβII is associated with the response to ischemia/reperfusion (I/R), though its role, either pathogenic or protective, has not been determined. In a murine model of single-lung I/R, evidence linking PKCβ to maladaptive responses is shown in the following studies. Homozygous PKCβ-null mice and WT mice fed the PKCβ inhibitor ruboxistaurin subjected to I/R displayed increased survival compared with controls. In PKCβ-null mice, phosphorylation of extracellular signal–regulated protein kinase-1 and -2 (ERK1/2), JNK, and p38 MAPK was suppressed in I/R. Expression of the immediate early gene, early growth response-1 (Egr-1), and its downstream target genes was significantly increased in WT mice in I/R, particularly in mononuclear phagocytes (MPs), whereas this expression was attenuated in PKCβ-null mice or WT mice fed ruboxistaurin. In vitro, hypoxia/reoxygenation-mediated induction of Egr-1 in MPs was suppressed by inhibition of PKCβ, ERK1/2, and JNK, but not by inhibition of p38 MAPK. These findings elucidate key roles for PKCβII activation in I/R by coordinated activation of MAPKs (ERK1/2, JNK) and Egr-1.

Introduction

Ischemic stress impacts broadly on cellular activation mechanisms, recruiting a number of central pathways such as hypoxia-inducible factor-1 (HIF-1) (1–3) and NF-κB (4–6). Although HIF-1α was linked to activation of the non–insulin-dependent glucose transporter (GLUT1) and expression of erythropoietin and VEGF (2–3, 7), previous studies demonstrated that early growth response-1–mediated (Egr-1–mediated) expression of tissue factor and deposition of fibrin in hypoxic vasculature was independent of HIF-1 (8). Furthermore, our studies delineated a previously unrecognized pathway in global hypoxia involving rapid activation of PKCβII and leading, via a series of steps including activation of raf, extracellular signal–regulated protein kinase-1 and 2 (ERK1/2), and elk-1, to upregulation of Egr-1, particularly in mononuclear phagocytes (MPs) in the lung and in cultured MPs exposed to hypoxia in vitro (9, 10). Egr-1, in turn, influences expression of a diverse array of genes relevant to the pathobiology of ischemia. Specifically, homozygous Egr-1 null mice subjected to lung ischemia/reperfusion (I/R) displayed reduced expression of cytokines, chemokines, cell adherence molecules, and procoagulant cofactors associated with ischemic tissue injury, in parallel with enhanced animal survival and organ function (11).

The PKC family is a family of multifunctional isoenzymes — which may be activated by diacylglycerols and Ca^{2+} — that play a central role in signal transduction and intracellular crosstalk by phosphorylating at serine/threonine residues an array of substrates, including cell surface receptors, enzymes, contractile proteins, transcription factors, and other kinases (12). Activation of PKC, indicated by translocation from the cytosol to the plasma membrane, occurs in response to transient increases in diacylglycerols or exposure to phorbol esters or hypoxia (9). Our previous studies demonstrated that compared with exposure of WT PKCβ-bearing (*PKC*$\beta^{+/+}$) mice to global hypoxia, homozygous PKCβ null (*PKC*$\beta^{-/-}$) mice displayed a sharp reduction in expression of tissue factor transcripts and antigen in the lung, in parallel with reduced vascular fibrin deposition and significantly reduced transcripts, antigen, and nuclear translocation of Egr-1 (10).

Here, we sought to dissect the impact of PKCβ specifically in I/R, and to test the hypothesis that PKCβ regulates inflammatory/prothrombotic gene expression and tissue injury in I/R. To address these concepts, we used a murine model of single-lung I/R using *PKC*$\beta^{-/-}$ mice (13) and WT mice fed chow containing the PKCβ inhibitor ruboxistaurin (LY333531) (14–21). To delineate the precise link between PKCβ and activation of signal transduction pathways in I/R, we performed in vitro hypoxia/reoxygenation (H/R) studies in cultured rat alveolar MPs. We demonstrate for the first time that deletion or pharmacological blockade of PKCβ confers striking protection from injury in I/R. PKCβ regulates the expression of proinflammatory/prothrombotic mediators in I/R, at least in part through Egr-1.

Results

*Effect of PKC*β *on the consequences of lung I/R: enhanced survival and maintenance of vascular homeostatic mechanisms.* *PKC*$\beta^{-/-}$ mice in the C57BL/6 background were subjected to single-lung ischemia for 1 hour followed by reperfusion for 3 hours. Following this treatment was a test period of 1 hour during which time reperfusion to the uninstrumented lung was blocked, rendering the animal dependent on the I/R lung. Compared with *PKC*$\beta^{+/+}$ controls, deletion of the *PKC*β gene conferred enhanced survival of about threefold (survival was 67% in *PKC*$\beta^{-/-}$ mice and 22% in *PKC*$\beta^{+/+}$ mice; $P = 0.03$; Figure 1A). In parallel, leukocyte accumulation in I/R tissue, an important indication of impending tissue damage, was decreased

Nonstandard abbreviations used: activator protein-1 (AP-1); early growth response-1 (Egr-1); electrophoretic mobility shift analysis (EMSA); extracellular signal–regulated protein kinase-1 and -2 (ERK1/2); hypoxia-inducible factor-1 (HIF-1); hypoxia/reoxygenation (H/R); ischemia/reperfusion (I/R); macrophage inflammatory protein-2 (MIP-2); mononuclear phagocyte (MP); phospho-specific c-Jun (p-c-Jun); plasminogen activator inhibitor-1 (PAI-1).

Conflict of interest: The authors have declared that no conflict of interest exists.

Citation for this article: *J. Clin. Invest.* **113**:1615–1623 (2004). doi:10.1172/JCI200419225.

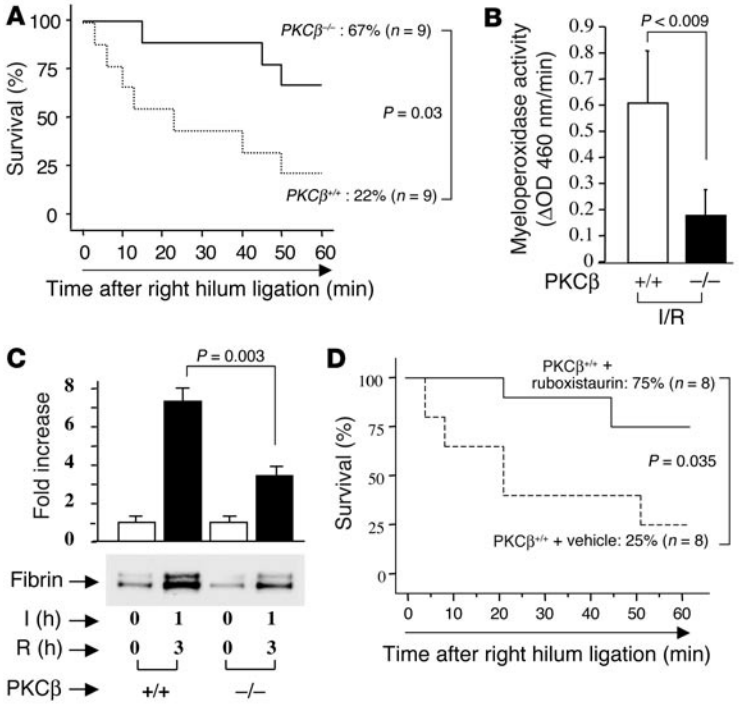

Figure 1
Murine model of lung ischemia/reperfusion (I/R): effect of PKCβ. (**A** and **D**) Survival analysis. *PKC*β$^{+/+}$ and *PKC*β$^{-/-}$ (**A**) and *PKC*β$^{+/+}$ mice fed vehicle chow or ruboxistaurin chow (**D**), respectively, were subjected to left-lung ischemia for 1 hour and reperfusion for 3 hours. Blood flow to the uninstrumented right lung was then blocked, and mortality was determined after 1 hour with only the left lung in the circulation. (**B**) Myeloperoxidase activity. After I/R, lung samples were harvested from *PKC*β$^{+/+}$ and *PKC*β$^{-/-}$ mice and subjected to myeloperoxidase activity assay ($n = 5$). (**C**) After left-lung I/R as described above, animals received systemic heparin and were sacrificed. Lung protein extract was digested with plasmin and subjected to SDS-PAGE (7.5%; 0.2 μg of total protein/lane). Immunoblotting with anti-fibrin antibody was performed. Data are shown as mean ± SEM of five experiments.

based on assessment of myeloperoxidase activity (Figure 1B). Pulmonary fibrin deposition, reflecting the balance of procoagulant and anticoagulant/fibrinolytic mechanisms in the injured lung, was significantly decreased in *PKC*β$^{-/-}$ mice compared with *PKC*β$^{+/+}$ mice, based on immunoblotting of lung extracts with an antibody directed to a fibrin neoepitope ($P = 0.003$, Figure 1C). Consistent with the apparently protective phenotype in *PKC*β$^{-/-}$ mice subjected to lung I/R, WT mice fed the PKCβ inhibitor ruboxistaurin (LY333531) that were subjected to lung I/R also displayed increased survival (about threefold; $P = 0.035$; Figure 1D). Taken together, these data indicate that deletion or blockade of PKCβ resulted in maintenance of vascular homeostatic mechanisms.

*Activation of PKC*β*II in response to lung I/R.* When WT C57BL/6 mice were subjected to I/R, rapid translocation of PKCβII to the cell membrane was observed, consistent with its activation. An increase of PKCβII associated with the membrane fraction reached an apparent maximum after 1 hour of ischemia and 10–15 minutes of reperfusion (Figure 2A). These studies were performed using an antibody selective to the PKCβII isoform. In contrast, immunoblotting with an antibody specific to the PKCβI isoform showed no change (not shown). Next, we examined the patterns of two other isoforms of PKC linked to I/R, PKCδ and PKCε. PKCδ and PKCε antigens in the membranous fraction from *PKC*β$^{+/+}$ and *PKC*β$^{-/-}$ mice showed no changes resulting from 15 minutes of reperfusion after 1 hour of ischemia (Figure 2, B and C), thus confirming that the activated principal isoform of PKC relevant to I/R injury in the lung was the PKCβII isoform.

*Activation of PKC*β*II upregulates expression of downstream MAPKs.* In view of the observed close relationship between environmental stress and PKCβII translocation, we considered what impact deletion of PKCβII in I/R might have on MAPKs ERK1 and ERK2 (p44 and p42), which are indirect downstream targets of this PKC isoform (9, 10, 22). Immunoblotting of extracts from I/R lung harvested from *PKC*β$^{+/+}$ mice displayed an approximately eightfold increase in intensity of phospho-p44/42 in samples from I/R lung compared with samples from uninstrumented lung (Figure 3A). In comparison, *PKC*β$^{-/-}$ mice displayed an increase of only about threefold in phosphorylation of p44/42 in I/R lung compared with tissue from uninstrumented lung (Figure 3A). Levels of total p44/42 antigen did not change in any of these experiments (Figure 3A). Immunostaining with antibody to phospho-p44/42 demonstrated increase of this epitope in the lung from *PKC*β$^{+/+}$ mice subjected to I/R (Figure 3C), compared with the uninstrumented lung, in which it was undetectable. However, in *PKC*β$^{-/-}$ mice, there was a slight increase in immunoreactive

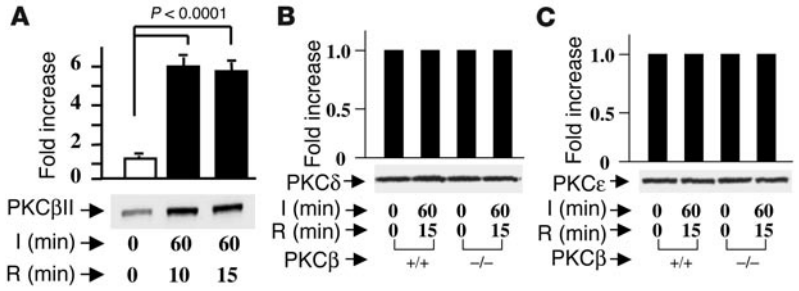

Figure 2
I/R-mediated activation of PKCβII in the lung. *PKC*β$^{+/+}$ and *PKC*β$^{-/-}$ mice were subjected to left-lung ischemia for 1 hour and reperfusion for 10–15 minutes. Membranous fractions were prepared from I/R and uninstrumented lung, and were subjected to SDS-PAGE (7.5%, 5 μg of total protein/lane) and immunoblotting with antibody to PKCβII (**A**), PKCδ (**B**), and PKCε (**C**).

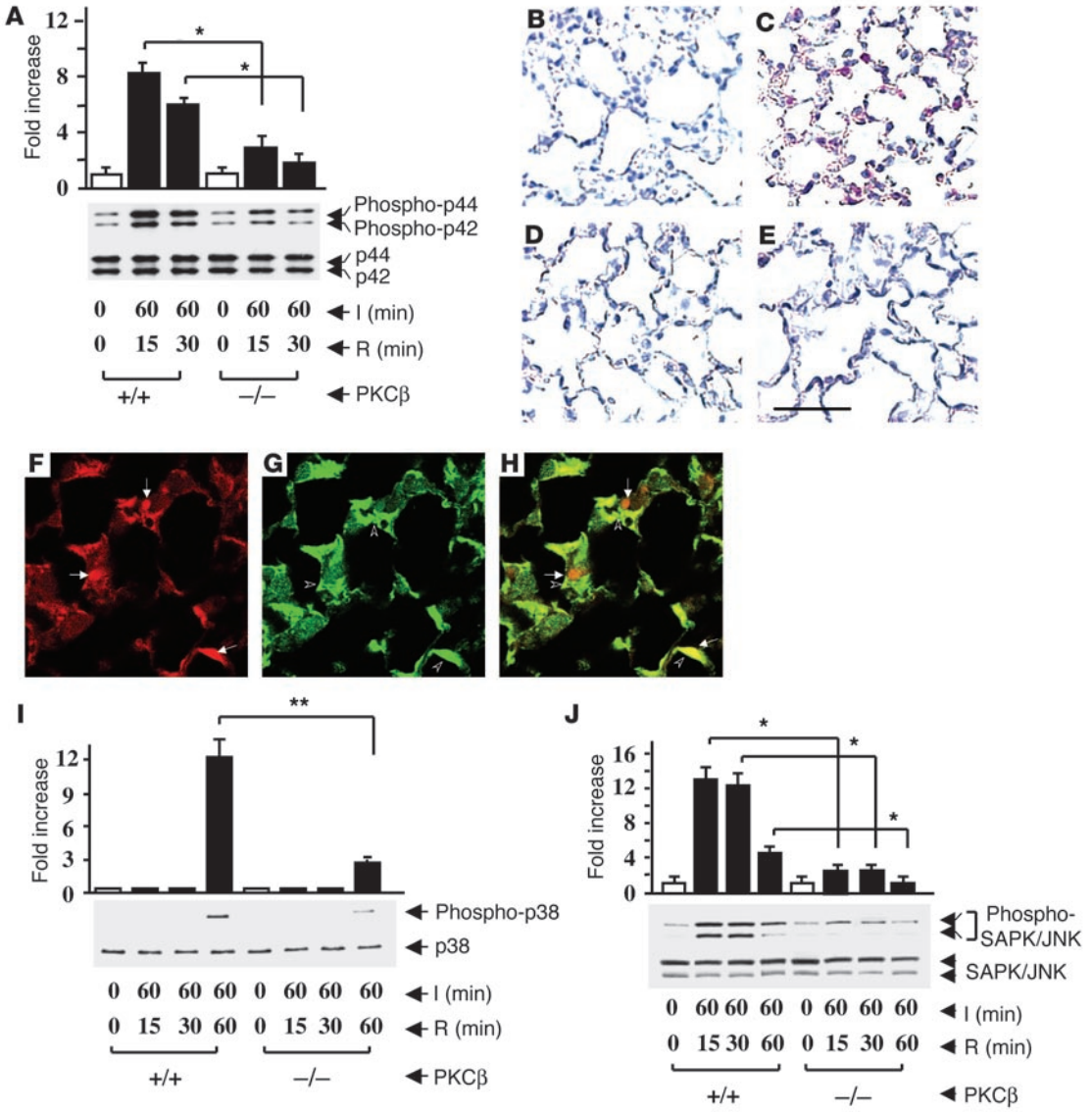

Figure 3

Ischemia/reperfusion-mediated activation of MAPKs in the lung. *PKC*β$^{+/+}$ and *PKC*β$^{-/-}$ mice underwent the indicated period of left-lung I/R. Animals were sacrificed and protein extracts from the I/R and uninstrumented lung were prepared and subjected to SDS-PAGE (12%, 50 μg of protein/lane). Immunoblotting with phospho-p44/42 MAPK antibody or total p44/42 MAPK antibody (**B**), phospho-p38 MAPK antibody, or total p38 MAPK antibody (**I**), and phospho-SAPK/JNK antibody or total SAPK/JNK antibody (**J**) was performed. Data are shown as mean ± SEM of five experiments. Immunohistochemical analysis of phospho-p44/42 expression in murine lung from uninstrumented (**B**) or I/R (**C**) *PKC*β$^{+/+}$ mice, and from uninstrumented (**D**) or I/R (**E**) *PKC*β$^{-/-}$ mice was performed. Scale bar: 50 μm. I/R lungs from *PKC*β$^{+/+}$ mice were subjected to immunofluorescence microscopy and double stained with an anti–phospho-p44/42 antibody (red) (**F**) and an anti-macrophage antibody (F4/80, green) (**G**). The merging of **F** (pERK1/2) and **G** (F4/80) is shown in **H**. Arrows in **F** and arrowheads in **G** indicate dually stained cells Original magnification in **F**–**H**, ×1,000. *$P < 0.001$; **$P = 0.0041$.

phospho-p44/42 in I/R lung (Figure 3E) that was similar to that of immunoreactive phospho-p44/42 in the lungs of uninstrumented *PKC*β$^{-/-}$ mice (Figure 3D). In addition, immunofluorescence of *PKC*β$^{+/+}$ I/R lung sections stained with anti–phospho-p44/42 and F4/80 IgG demonstrated that phospho-p44/42 antigen was localized predominantly in MPs. Figure 3F demonstrates staining with anti–phospho-p44/42 kinase (red), and Figure 3G demonstrates staining using anti-F4/80 IgG (green) to identify MPs. Figure 3H reveals the merge and indicates that phospho-p44/42 MAPK is, at least in part, expressed in MPs in the I/R lung.

These data led us to consider the effect of deleting PKCβ on other MAPKs, each of which has been implicated in inflammatory responses to cell stress. Immunoblotting of lung extracts was performed with an antibody selective for phospho-p38 (Figure 3I). An about 13-fold increase in intensity of the phospho-p38 band was observed in I/R lung from *PKC*β$^{+/+}$ mice compared with uninstrumented lung from *PKC*β$^{+/+}$ mice (Figure 3I). Immunohistochemical studies demonstrated that increased phospho-p38 was present predominantly in MPs following I/R of *PKC*β$^{+/+}$ mouse lung, compared with uninstrumented controls, in which it was undetectable

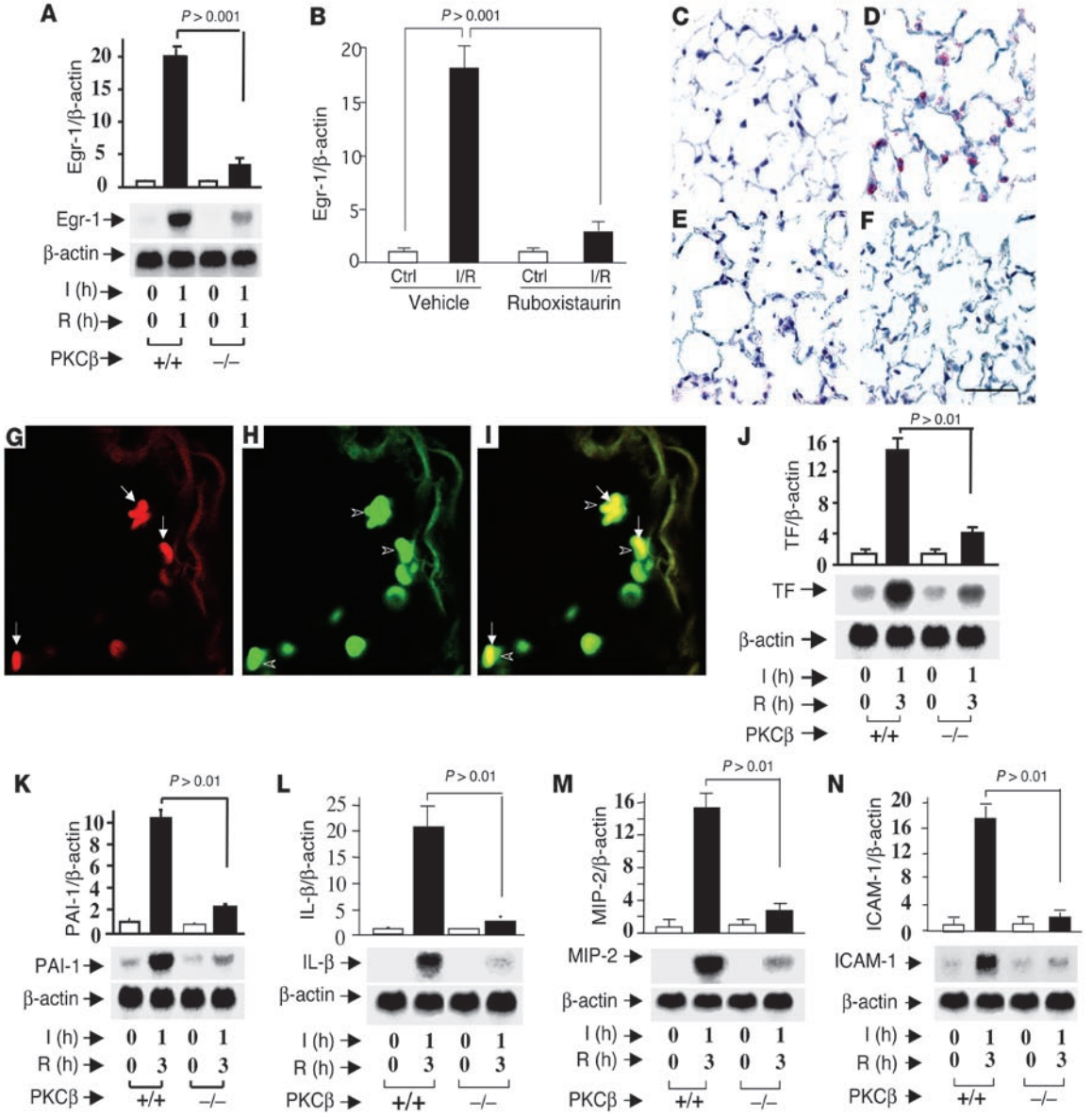

Figure 4

I/R induces Egr-1 and procoagulant and proinflammatory molecules in the lung: effect of PKCβ. Mice underwent left lung I/R or no instrumentation. Mice were sacrificed and total RNA was isolated from the lung and subjected to Northern analysis (20 μg/lane) with ^{32}P-labeled cDNA probes for Egr-1 (**A**), tissue factor (TF) (**J**), PAI-1 (**K**), IL-1β (**L**), MIP-2 (**M**), ICAM-1 (**N**), or β-actin (as internal control). Real-time PCR analysis of total RNA for Egr-1 expression was performed on I/R and uninstrumented lungs from WT mice fed vehicle or ruboxistaurin chow (**B**). Immunohistochemical analysis of Egr-1 expression in murine lung from uninstrumented (**C**) or I/R (**D**) *PKC*β$^{+/+}$ mice and from uninstrumented (**E**) or I/R (**F**) *PKC*β$^{-/-}$ mice. Ctrl, control. Scale bar in **F**: 50 μM. I/R lungs from *PKC*β$^{+/+}$ mice were immunofluorescence double stained with an anti–Egr-1 antibody (red) (**G**) and an anti-MP antibody (F4/80, green) (**H**). The merging of **G** (Egr-1) and **H** (F4/80) is shown in **I**. Arrows in **G** and arrowheads in **H** indicate dually stained cells. Original magnification in **G**–**I**, ×1,000. The units for the *y* axes of **A**, **B**, and **J**–**N** are fold increase.

(not shown). However, in *PKC*β$^{-/-}$ mice, phosphorylation of p38 after I/R was suppressed (about fourfold) compared with *PKC*β$^{+/+}$ mice undergoing I/R (Figure 3I). Similarly, there was an increase in intensity of about 13-fold of the phospho-SAPK/JNK band in extracts from I/R lung compared with the uninstrumented lung from *PKC*β$^{+/+}$ mice (Figure 3J). In contrast, the increase in phospho-SAPK/JNK band was considerably blunted in I/R lung from *PKC*β$^{-/-}$ animals (~2.5-fold, compared with uninstrumented control *PKC*β$^{-/-}$ mice). In addition, immunohistochemical studies demonstrated that increased phospho-SAPK/JNK were present predominantly in MPs (not shown). Taken together, these data show decreased activation of phospho-p44/42, phospho-p38, and phospho-SAPK/JNK of about 70% ($P < 0.001$), 77% ($P = 0.004$), and 75% ($P < 0.001$), respectively, in I/R lung from *PKC*β$^{-/-}$ compared with I/R lung from *PKC*β$^{+/+}$ mice.

*Effect of PKC*β *gene deletion on targets of MAPKs.* Since expression of Egr-1 has been linked to PKCβ-dependent MAPK activity in global hypoxia (9, 10), we tested the role of PKCβ in modulating

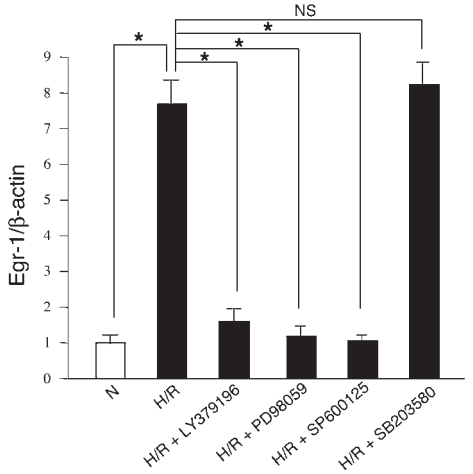

Figure 5
H/R-mediated induction of Egr-1 in rat alveolar MPs (NR8383): effect of inhibitors of PKCβ and MAPKs. Rat MPs were incubated with LY379196 (200 nM), PD98059 (50 μM), SP600125 (20 μM), and SB203580 (10 μM), respectively, for 1 hour before being subjected to hypoxia for 30 minutes followed by reoxygenation for 15 minutes. Comparison is with H/R alone or normoxia (N). Real-time PCR analysis of total RNA from the above cells was performed. Data are presented as the fold induction of mRNA for Egr-1 normalized to β-actin. These experiments were repeated five times. *$P < 0.001$.

expression of Egr-1 specifically in I/R. Transcripts for Egr-1 were increased by 18- to 20-fold in I/R lung from *PKC*β$^{+/+}$ mice compared with Egr-1 transcripts from uninstrumented *PKC*β$^{+/+}$ animals (Figure 4, A and B). In contrast, I/R in *PKC*β$^{-/-}$ mice (Figure 4A) or WT mice fed PKCβ inhibitor ruboxistaurin (Figure 4B) caused only a two- to threefold increase in Egr-1 mRNA transcripts. At the protein level, immunohistochemical analysis for Egr-1 antigen demonstrated a strong increase of antigen in lungs from *PKC*β$^{+/+}$ mice subjected to I/R (Figure 4D) compared with uninstrumented controls (Figure 4C). Immunoreactivity for Egr-1 antigen was largely expressed in MPs, as demonstrated by using immunofluorescence to colocalize Egr-1 in MPs using antibodies to Egr-1 (Figure 4G, red) and anti-F4/80 IgG (Figure 4H, green). Figure 4I represents the merge, indicating that Egr-1 was principally expressed in MPs in *PKC*β$^{+/+}$ I/R lung. In contrast to these findings in *PKC*β$^{+/+}$ mice, in *PKC*β$^{-/-}$ mice there was only a slight increase in immunoreactive Egr-1 in I/R lung (Figure 4F), which was not significantly different from that observed in uninstrumented lung retrieved from *PKC*β$^{-/-}$ mice (Figure 4E).

We next examined the impact of PKCβ on expression of proinflammatory/prothrombotic genes in IR. Previous studies revealed that Egr-1 regulated a broad array of such mediators in I/R (11). Compared with *PKC*β$^{+/+}$ mice, factors regulating the vascular coagulant environment, such as tissue factor and plasminogen activator inhibitor-1 (PAI-1), displayed only a slight increase in transcripts in *PKC*β$^{-/-}$ mice. Levels of tissue factor and PAI-1 mRNA were increased by 15- and tenfold, respectively, in I/R lung from *PKC*β$^{+/+}$ mice compared with uninstrumented *PKC*β$^{+/+}$ controls (Figure 4, J and K). In *PKC*β$^{-/-}$ mice, tissue factor and PAI-1 mRNA were enhanced only by about fourfold and twofold, respectively, in the I/R lung. The same pattern of gene expression was observed comparing *PKC*β$^{-/-}$ and *PKC*β$^{+/+}$ mice with respect to I/R-induced upregulation of proinflammatory cytokines (IL-1β), chemokines (macrophage inflammatory protein-2, MIP-2), and ICAM-1 (Figure 4, L, M, and N). Whereas IL-1β, MIP-2, and ICAM-1 displayed robust induction of transcripts in I/R lung from *PKC*β$^{+/+}$ mice (increases of 20-, 16-, and 18-fold, respectively), these increases were much less prominent in I/R lungs from *PKC*β$^{-/-}$ mice (increases of approximately two-, three-, and twofold, respectively). In each case, the differences between enhanced levels of transcripts for these genes in I/R lungs from *PKC*β$^{+/+}$ and *PKC*β$^{-/-}$ mice were statistically significant ($P < 0.01$ for tissue factor, PAI-1, IL-1β, MIP-2, and ICAM-1, respectively).

*Mechanisms of I/R-induced PKC*β*-dependent signaling pathways.* These considerations provide important insights into the potential downstream consequences of PKCβ-dependent activation of these multifaceted signaling cascades after I/R. The lack of orally administered inhibitors (or ready-made chow containing such inhibitors) of the three MAPKs (ERK1/2, JNK, or p38) for chronic administration to animals in vivo renders it difficult to directly assess the impact of these kinases on downstream targets. However, inhibitors of ERK1/2 (PD98059), JNK (SP600125), and p38 (SB203580) are available and suitable for in vitro studies. Therefore, to dissect the molecular mechanisms by which PKCβ activation upregulated Egr-1 in I/R, we used a rat alveolar MP cell line (NR8383), since alveolar MPs prominently displayed MAPKs such as phospho-ERK1/2 and Egr-1 in I/R lung. H/R was chosen as an in vitro model system to mimic key components of the ischemic/reperfused vascular milieu. Cultured MPs were serum-starved for 24 hours and exposed to hypoxia (oxygen pressure, 14 torr) for 30 minutes, then reoxygenation for 15 minutes. Real-time PCR analysis of total RNA from H/R MPs demonstrated an approximate eightfold increase in Egr-1 transcripts compared with normoxic MPs ($P < 0.001$) (Figure 5), in a manner strikingly suppressed by the inhibitor of PKCβ (LY379196, 200 nM; displays similar K_i for the βI and βII isoforms [refs. 23, 24]). The increase in Egr-1 transcripts in H/R was also strongly suppressed by the inhibitors of ERK1/2 (PD98059, 50 μM) and JNK (SP600125, 20 μM) but not by an inhibitor of p38 (SB203580, 10 μM)] (Figure 5). These findings suggest that the PKCβ pathway modulates Egr-1 upregulation via phosphorylation of ERK1/2 and JNK, but not via phosphorylation of p38 in MPs in response to I/R injury.

*Activation of transcription factors activator protein-1 and NF-*κ*B in I/R: effect of PKC*β. Lastly, we addressed the question of whether other key transcriptional regulatory pathways, such as activator protein-1 (AP-1) or NF-κB, were modulated by PKCβ in I/R beyond Egr-1. Compared with WT mice, *Egr1*$^{-/-}$ mice subjected to I/R did not reveal modulation of AP-1 or NF-κB DNA binding (data not shown). Thus, the possibility that PKCβ might modulate these pathways in I/R was important to consider, as activation of AP-1 (25) and NF-κB (26) have been shown in cells in response to hypoxia or hydrogen peroxide stress. Therefore, we investigated induction of AP-1 and NF-κB DNA binding activities in I/R lung from *PKC*β$^{+/+}$ and *PKC*β$^{-/-}$ mice. Electrophoretic mobility shift analysis (EMSA) for AP-1 DNA binding activity, using a ^{32}P-labeled consensus AP-1 oligonucleotide and nuclear extract from I/R lung derived from WT animals, showed induction of a prominent gel shift band (Figure 6A, compare lane 3 with lane 2, showing about an 11-fold increase in band intensity with I/R). This I/R-induced gel shift band represented specific binding to the AP-1 probe, as demonstrated by competition experiments; excess unlabeled AP-1 oligonucleotide blocked appearance of the band, whereas an unrelated Sp1 probe was without effect (lane 7 and lane 6 in Figure 6A). The observa-

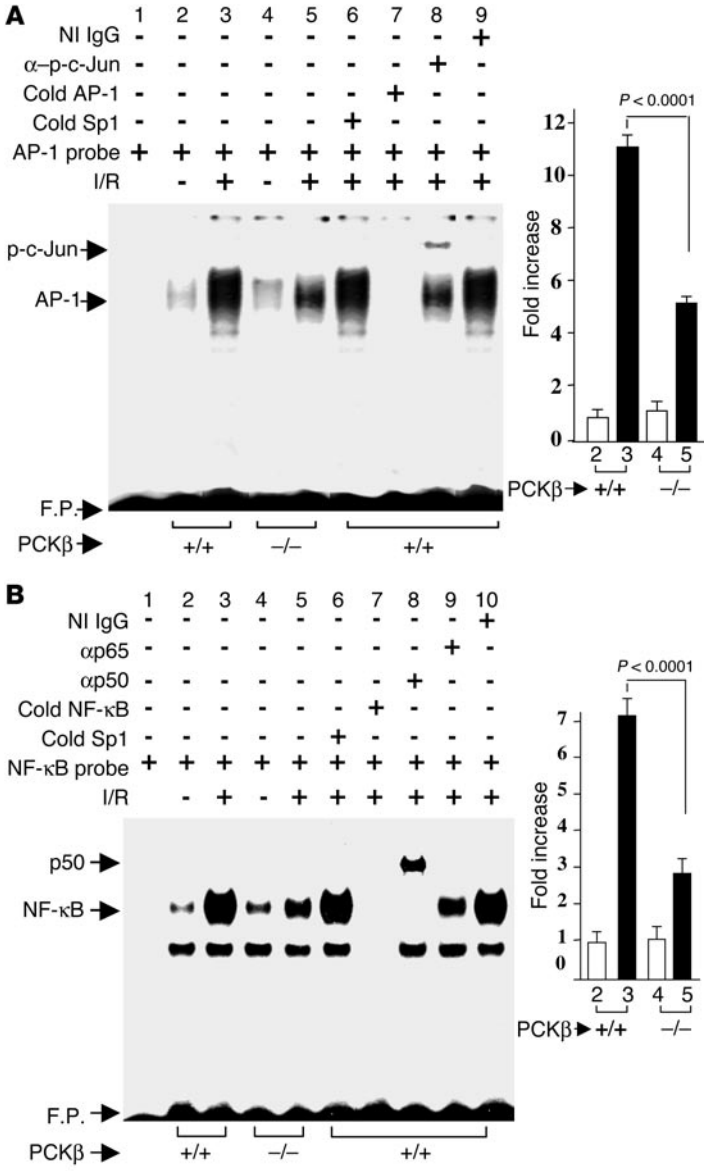

Figure 6
I/R-mediated induction of AP-1 and NF-κB in the lung: effect of PKCβ. Mice underwent left-lung I/R or no instrumentation. Mice were sacrificed, and nuclear extracts were prepared from the lung and subjected to EMSA with ^{32}P-labeled consensus AP-1 (**A**) and NF-κB (**B**) probes. Where indicated, nuclear extracts from uninstrumented (lane 2 and lane 4) and I/R (lane 3 and lane 5) lung were incubated with ^{32}P-labeled AP-1 (**A**) or NF-κB (**B**) probe alone. Nuclear extracts from I/R lungs of *PKC*β$^{+/+}$ mice were incubated with ^{32}P-labeled AP-1 (**A**) or NF-κB (**B**) probe in the presence of either a 100-fold molar excess of Sp1 (cold Sp1; lane 6 in **A** and **B**), AP-1 (cold AP-1; lane 7 in **A**), or NF-κB (cold NF-κB; lane 7 in **B**), and either anti–p-c-Jun IgG (lane 8 in **A**), anti-p50 IgG (lane 8 in **B**), and anti-p65 IgG (lane 9 in **B**) or nonimmune (NI) IgG (lane 9 in **A** and lane 10 in **B**, respectively). F.P., free probe.

tion that incubation with antibody to phospho-specific c-Jun (p-c-Jun) resulted in a supershift of the band corresponding to AP-1 DNA binding activity (Figure 6A, lane 8; lane 9 shows nonimmune IgG) indicated the involvement of this protein in the AP-1 complex. However, antibody to c-Fos had no effect in this supershift assay (data not shown). In contrast, when nuclear extracts were prepared from *PKC*β$^{-/-}$ mice subjected to I/R, intensity of the AP-1 gel shift band was significantly attenuated (Figure 6A, $P < 0.0001$, compare lane 5 with lane 3) compared with AP-1 after I/R in WT mice.

In addition, EMSA with a ^{32}P-labeled NF-κB probe and nuclear extracts from I/R lung harvested from WT mice demonstrated a 7.3-fold increase in band intensity compared with uninstrumented lung (Figure 6B, compare lane 3 with lane 2). The issue of specificity was addressed by competition studies in which excess unlabeled NF-κB probe blocked appearance of the gel shift band, whereas excess of another unrelated probe, Sp1, was without effect (Figure 6B, lane 7 and lane 6, respectively). Supershift analysis showed the presence of NF-κB p50 and p65 in the gel shift complex (Figure 6B, lane 8 and lane 9; lane 10 shows nonimmune IgG). When similar experiments were performed with nuclear extracts from I/R lung harvested from *PKC*β$^{-/-}$ mice, the intensity of the gel shift band was strikingly reduced compared with that produced using I/R *PKC*β$^{+/+}$ mice (Figure 6B, compare lane 5 with lane 3; $P < 0.0001$). These data indicated that modulation of AP-1 or NF-κB activation was dependent on PKCβ, and not Egr-1, in the I/R lung.

Discussion

These data provide the first evidence that PKCβII activation, which begins early in the reperfusion period, plays a pivotal role in the pathogenesis of I/R lung injury. These studies highlight a new facet to the biology of PKCβII in I/R, and are especially relevant in view of the enhanced protection afforded by either genetic deletion or pharmacological blockade of PKCβ with ruboxistaurin (a threefold increase in survival) versus that observed in homozygous *Egr-1*$^{-/-}$ mice (a twofold increase in survival) (11).

In the present study, we showed that in parallel with enhanced animal survival and maintenance of vascular homeostasis, deletion of PKCβ in I/R significantly impacted pathways leading to phosphorylation of ERK1/2, JNK, and p38 MAPKs, and ultimately to expression of transcription factors Egr-1, AP-1, and NF-κB and their downstream targets. Hypoxemia, a central component of the vascular milieu manifest at the earliest time in ischemic disorders, is a logical potential trigger for vascular perturbation. Therefore, the mechanism of activation of PKCβ-dependent activation of ERK1/2 and the consequent upregulation of the Egr-1 pathway in I/R-triggered stress is consistent with our previous studies of global hypoxemic stress in vitro (9) and in vivo (10). In addition, the current results in *PKC*β$^{-/-}$ mice confirm the broad outlines of this pathway and underscore the concept that, in addition to upregulation of ERK1/2, PKCβ is also an early and key trigger to the activation of JNK and p38 MAPKs that occurs in response to I/R. Consistent with our findings, it has been reported that activation of JNK and/or p38 MAPK appeared in the heart or kidney exposed to I/R, and in cardiac myocytes subjected to H/R (27–33). It is highly likely that the pattern and time course of ERK, JNK, and p38 MAPK activation are tissue-specific (29, 34, 35).

Interestingly, our observations elucidated that these signal transduction mechanisms may contribute to cellular responses to

ischemic stresses, such as induction of inflammation and coagulation. The coagulant properties of alveolar macrophages are likely to be relevant to the procoagulant environment of hypoxemic lung. In our previous study with monocyte-like U937 cells, hypoxia was shown to induce membrane translocation and autophosphorylation of PKCβII, compared with lack of such changes in PKC isoforms α and ε (9). Furthermore, transient transfection studies demonstrated that expression of dominant-negative PKCβII selectively suppressed hypoxia-mediated activation of Egr-1 and tissue factor transcription (9). In the present studies, we demonstrated that the activated principal isoform of PKC relevant to I/R lung injury was specifically PKCβII, not PKCβI, PKCδ, or PKCε. These data suggest that the activation of individual PKC isoforms in ischemia or I/R is clearly tissue-specific, as previous studies have demonstrated activation of PKCδ and PKCε in ischemia or I/R in the heart (36–38).

In addition, these studies have outlined a pathway in MPs whereby activation of PKCβ-dependent signaling pathways in hypoxia/reoxygenation leading to upregulation of Egr-1 transcripts was via phosphorylation of specific MAPKs. Previous studies by others have used the PKCβ inhibitor LY333531 in a porcine model of ischemia-induced preretinal neovascularization (17) and in diabetic rats to ameliorate, at least in part, early retinal and renal dysfunction (15). Here, we have provided the first evidence that administration of ruboxistaurin suppressed upregulation of Egr-1 transcripts upon I/R. The lack of availability of agents to inhibit the three MAPKs (ERK1/2, JNK, and p38) in vivo in this model renders it difficult to precisely link PKCβ-dependent activation of these pathways to recruitment/stimulation of downstream targets. However, we have provided evidence that suppressed expression of Egr-1 in vitro in H/R was achieved by preincubation of alveolar MPs with inhibitors of PKCβ (LY379196), ERK1/2 (PD98059), and JNK (SP600125) prior to exposure to H/R, but not by an inhibitor of p38 MAPK (SB203580).

Although the activities of NF-κB and AP-1 may be modulated and regulated by a complex interaction between ERK1/2, JNK, and p38 MAPK pathways (39, 40), our data provide the first evidence that PKCβ modulated activation of AP-1 and NF-κB in response to I/R injury. Importantly, the lack of modulation of AP-1 or NF-κB in *Egr-1*$^{-/-}$ mice in lung I/R suggests that the biologic impact of PKCβ in I/R may exceed its effects solely on regulation of Egr-1. The exact mechanisms and signaling pathways by which PKCβ modulates activation of AP-1 and NF-κB in I/R are not yet known, but are the subject of ongoing investigation.

In conclusion, these findings delineate novel roles for PKCβ in I/R injury. The observation that activation of PKCβ-dependent signaling regulates recruitment of proinflammatory and prothrombotic mechanisms highlights new targets for the prevention of organ dysfunction and damage in disorders characterized by I/R injury.

Methods

*Murine model of I/R. PKC*β$^{-/-}$ mice (13) have been backcrossed more than ten generations into C57BL/6 in our laboratory. WT C57BL/6 mice were purchased from The Jackson Laboratory (Bar Harbor, Maine, USA). Both *PKC*β$^{-/-}$ mice and *PKC*β$^{+/+}$ controls (8–12 weeks old) were subjected to the single-lung I/R procedure according to protocols approved by the Institutional Animal Care and Use Committee at Columbia University. Left-lung ischemia was performed as described (41). In addition, C57BL/6 mice were fed chow containing the PKCβ inhibitor ruboxistaurin (LY333531; 10 mg/kg daily) from 3 days prior to I/R to the time of sacrifice.

Survival experiments. The surgical operator was blinded to mouse genotype. After 1 hour of ischemia, followed by 3 hours of reperfusion, the contralateral (right) hilum was permanently ligated, so that survival and gas exchange depended solely on the reperfused left lung for 1 hour. Survival during this period was defined as described (41). Arterial blood gas analysis (sampled from the left ventricle) was performed in mice who survived the 1-hour period after right hilar ligation.

Analysis of myeloperoxidase activity. Lungs were homogenized in detergent containing hexadecyltrimethylammonium bromide, freeze-thawed, and centrifuged, and supernatants were assayed for myeloperoxidase activity using substrate buffer containing *o*-dianisidine (42). Myeloperoxidase activity was measured at an absorbance of 460 nm for 20 seconds and calculated as ΔOD 460 nm/min using a UV/visible spectrophotometer (Ultrospec 3000; Amersham Biosciences, Piscataway, New Jersey, USA).

Western-blot analysis. Fibrin levels were determined in lungs extracted from animals treated with heparin (10 U/g body wt, resulting in an activated partial thromboplastin time > 300 s) prior to sacrifice (43). Tissue was subjected to immunoblotting with anti-fibrin antibody as described (8, 44). To detect PKCβ isoforms I and II, PKCδ, and PKCε, cytosolic and membrane protein fractions were prepared from lung as described (9, 45). To detect ERK1/2, p38, and JNK, total protein extracts were prepared from lung tissue using cell lysis buffer (Cell Signaling Technology Inc., Beverly, Massachusetts, USA). Particulate material was removed by centrifugation, and protein concentration was determined using the Bio-Rad protein assay (Bio-Rad Laboratories Inc., Hercules, California, USA). Equal amounts of total protein (20 μg/sample) were subjected to SDS-PAGE (7.5% or 12%) followed by electrophoretic transfer to nitrocellulose membranes (46). Nonspecific binding was blocked by incubation of membranes with nonfat dry milk or BSA (5%) for 1 hour at room temperature or overnight at 4°C. To detect membrane protein translocation, each blot was incubated with one of the following first antibodies: anti-PKCβI IgG, anti-PKCβII IgG, anti-PKCδ IgG, or anti-PKCε IgG (Santa Cruz Biotechnology Inc., Santa Cruz, California, USA). To detect MAPKs, each blot was incubated with one of the following antibodies as the first antibody for the reaction: anti–phospho-p44/42 IgG, anti–total-p44/42 IgG, anti–phospho-SAPK/JNK IgG, anti–total-SAPK/JNK IgG, anti-phospho-p38 IgG, or anti–total-p38 IgG (Cell Signaling Technology Inc.). Each first antibody was used at a dilution of 1:1,000 for 1–3 hours or overnight according to the manufacturer's instructions. HRP-conjugated donkey anti-rabbit IgG secondary antibody (1:2,000; Amersham Biosciences) was used to identify sites of binding of primary antibody.

Immunohistochemistry. Lung tissue was harvested and fixed in formalin and then embedded in paraffin. Sections were stained with the following primary antibodies: rabbit anti–Egr-1 IgG (8 μg/ml; Santa Cruz Biotechnology Inc.), rat F4/80 monoclonal antibody (10 μg/ml; PharMingen, San Diego, California, USA), rabbit anti–phospho- or total p44/42, p38, and SAPK/JNK IgG (1:10; Cell Signaling Technology Inc.) or nonimmune IgG, respectively. Secondary antibodies (affinity-purified alkaline phosphatase–conjugated anti-rabbit and anti-rat IgGs) and substrates were used as described (9, 10).

Immunofluorescence. Deparaffinized tissue sections were blocked with diluted normal blocking serum and incubated with a rabbit polyclonal anti–mouse Egr-1 antibody (1:40; Santa Cruz Biotechnology Inc.) or a rabbit anti–phospho-p44/42 antibody (1:250; Cell Signaling Technology Inc.), and then incubated with a biotinylated

goat anti-rabbit IgG (1:200; Vector Laboratories Inc., Burlingame, California, USA) followed by incubation with Texas Red–avidin D. The sections were blocked with avidin/biotin blocking solution according to the manufacturer's instructions (Vector Laboratories Inc.). The sections were then incubated with a rat monoclonal anti-mouse macrophage F4/80 antibody (1:10; PharMingen), and incubated with a biotinylated rabbit anti-rat IgG (1:200; Vector Laboratories Inc.) followed by fluorescein–avidin D. For confocal microscopy, antigen detection was performed using a LaserSharp 2000 scanning confocal microscope with epifluorescent illumination (Bio-Rad Laboratories Inc.) (excitation wavelength 488 nm for fluorescein–avidin D, 568 nm for Texas Red–avidin D).

Northern analysis. Total RNA was extracted from lung, followed by electrophoresis, transfer to Duralon-UV membranes (Stratagene, La Jolla, California, USA), and hybridization with ^{32}P-labeled cDNA probes for mouse Egr-1, tissue factor, PAI-1, IL-1β, MIP-2, and ICAM-1 as described (11). Northern blots were also hybridized with ^{32}P-labeled β-actin as an internal control for RNA loading. Autoradiograms were analyzed by densitometric scanning from at least three different experiments (a representative autoradiogram is shown in the figures). Absorption values were normalized to the β-actin band.

EMSA. Nuclear extracts were isolated from lung tissue as previously described (8). Double-stranded oligonucleotide probes for AP-1 and NF-κB (Promega Corp., Madison, Wisconsin, USA) were 5′ end–labeled with [^{32}P]ATP (3,000 Ci/mmol) using T4 polynucleotide kinase and standard procedures. Where indicated, antiserum to p-c-Jun, p50, p65, or nonimmune IgG was incubated with the nuclear extract at room temperature for 45 minutes, and then binding reactions and electrophoresis were performed as described (8). For competition studies, a 100-fold molar excess of unlabeled probes for either AP-1, NF-κB, or Sp1 (Promega Corp.) was added.

Cell culture. A rat alveolar macrophage cell line (NR8383) was obtained from American Type Culture Collection (Manassas, Virginia, USA), and cells were grown in Ham's F-12K medium containing 15% heat-inactivated FCS. Cells were made quiescent by serum starvation for 24 hours. Inhibitors of PKCβ (LY379196, 200 nM), ERK1/2 (PD98059, 50 μM), p38 (SB203580, 10 μM), and JNK (SP600125, 20 μM) were added 1 hour before induction of hypoxia. Using an environmental chamber as described previously (8), cells were subjected to 30 minutes of hypoxia (oxygen pressure in the medium was 12–14 torr). Cells subjected to hypoxia were placed in medium preequilibrated with the hypoxic gas mixture just prior to placement in the environmental chamber. Thus, cultures were immersed immediately in the oxygen-deprived environment at the time of medium change/placement in the chamber. After hypoxia, cells were placed in normal cell culture conditions for 15 minutes for reoxygenation.

Real-time quantitative PCR. Total RNA was extracted from lung or cells using Trizol reagent (Invitrogen Corp., Rockville Maryland, USA). Total RNA (1 μg) was processed directly to cDNA synthesis using the TaqMan Reverse Transcription Reagents kit (Applied Biosystems, Foster City, California, USA) according to the manufacturer's protocol. All PCR primers and TaqMan probes were designed using PrimerExpress software (Applied Biosystems) and published sequence data from the National Center for Biotechnology Information database. The sequences of forward and backward primers for rat Egr-1 are 5′-GGGAGCCGAGCGAACAA-3′ and 5′-CCAGCGCCTTCTCGTTATTC-3′, respectively. The sequences of forward and backward primers for rat β-actin are 5′-CCAGATCATGTTTGAGACCTTCAA-3′ and 5′-AGGGACAACACAGCCTGGAT-3′, respectively. The sequence of the TaqMan probe for rat Egr-1 is 5′-CTACGAGCACCTGACC-3′. The sequence of the TaqMan probe for rat β-actin is 5′-CCAGCCATGTACGTAGC-3′. Primers were synthesized, and TaqMan probes for rat Egr-1 or β-actin were labeled with the reporter dye 6FAM or VIC at the 5′ end, and Minor Groove Binder (MGB) attached at the 3′ end (all from Applied Biosystems). All reactions were performed in triplicate in the ABI PRISM 7900HT Sequence Detection System (Applied Biosystems). β-Actin was used as an active and endogenous reference to correct for differences in the amount of total RNA added to the reaction mixture and to compensate for different levels of inhibition during reverse transcription of RNA and during PCR. Data are calculated by the $2^{-\Delta\Delta CT}$ method (47) and are presented as the fold induction of mRNA for Egr-1 in I/R lungs or H/R MPs normalized to β-actin, compared with uninstrumented lungs or normoxic MPs (defined as 1.0-fold in each case).

Statistical analysis. All data are reported as mean ± SEM. Myeloperoxidase activity data were analyzed using the Mann-Whitney *U* test for unpaired variables. Animal survival after lung I/R was evaluated by contingency analysis using the χ^2 statistic. All analyses were performed using the StatView statistical package (version 5.0.1). To determine statistical significance, the Student unpaired *t* test was used for comparison between groups. ANOVA with post-hoc analysis with the Bonferroni/Dunn test was used to compare three or more groups. *P* values of less than 0.05 were considered statistically significant.

Acknowledgments

The authors gratefully acknowledge support from the LeDucq Foundation, the Surgical Research Fund of Columbia University, the Burroughs Wellcome Fund, and grants from the United States Public Health Service (USPHS). A.M. Schmidt is a recipient of a Burroughs Wellcome Fund Clinical Scientist Award in Translational Research.

Received for publication June 17, 2003, and accepted in revised form March 29, 2004.

Address correspondence to: Shi-Fang Yan, BB1705, Department of Surgery, College of Physicians and Surgeons of Columbia University, 630 West 168th Street, New York, New York 10032, USA. Phone: (212) 305-6030; Fax: (212) 305-5337; E-mail: sy18@columbia.edu.

1. Semenza, G.L. 2000. Surviving ischemia: adaptive responses mediated by hypoxia-inducible factor 1. *J. Clin. Invest.* **106**:809–812.
2. Zhu, H., and Bunn, H. 1999. Oxygen sensing and signaling impact on the regulation of physiologically important genes. *Respir. Physiol.* **115**:239–247.
3. Ratcliffe, P., et al. 1998. Oxygen sensing, HIF-1 and the regulation of mammalian gene expression. *J. Exp. Biol.* **201**:1153–1162.
4. Karakurum, M., et al. 1994. Hypoxic induction of interleukin-8 gene expression in human endothelial cells. *J. Clin. Invest.* **93**:1564–1570.
5. Royds, J., et al. 1998. Response of tumour cells to hypoxia: role of p53 and NFkB. *Mol. Pathol.* **51**:55–61.
6. Schmedtje, J., et al. 1997. Hypoxia induces cyclooxygenase-2 via the NF-kappaB p65 transcription factor in human vascular endothelial cells. *J. Biol. Chem.* **272**:601–608.
7. Semenza, G. 1999. Perspectives on oxygen sensing. *Cell.* **98**:281–284.
8. Yan, S.F., et al. 1998. Tissue factor transcription driven by Egr-1 is a critical mechanism of murine pulmonary fibrin deposition in hypoxia. *Proc. Natl. Acad. Sci. U. S. A.* **95**:8298–8303.
9. Yan, S.F., et al. 1999. Hypoxia-associated induction of early growth response-1 gene expression. *J. Biol. Chem.* **274**:15030–15040.
10. Yan, S.F., et al. 2000. Protein kinase C-β and oxygen deprivation. A novel Egr-1-dependent pathway for fibrin deposition in hypoxemic vasculature. *J. Biol. Chem.* **275**:11921–11928.
11. Yan, S.F., et al. 2000. Egr-1, a master switch coor-

dinating upregulation of divergent gene families underlying ischemic stress. *Nat. Med.* **6**:1355–1361.
12. Idris, I., Gray, S., and Donnelly, R. 2001. Protein kinase C activation: isozyme-specific effects on metabolism and cardiovascular complications in diabetes. *Diabetologia.* **44**:659–673.
13. Leitges, M., et al. 1996. Immunodeficiency in protein kinase Cβ deficient mice. *Science.* **273**:788–791.
14. Ceolotto, G., et al. 1999. Protein kinase C activity is acutely regulated by plasma glucose concentration in human monocytes in vivo. *Diabetes.* **48**:1316–1322.
15. Aiello, L.P., et al. 1997. Vascular endothelial growth factor induced retinal permeability is mediated by PKC in vivo and suppressed by an orally effective β-isoform selective inhibitor. *Diabetes.* **46**:1473–1480.
16. Ishii, H., et al. 1996. Amelioration of vascular dysfunction in diabetic rats by an oral PKCβ inhibitor. *Science.* **272**:728–731.
17. Bursell, S.E., et al. 1997. Specific retinal DAG and PKCβ isoform modulation mimics abnormal retinal hemodynamics in diabetic rats. *Invest. Ophthalmol. Vis. Sci.* **38**:2711–2720.
18. Danis, R.P., Bingaman, D.P., Jirousek, M., and Yang, Y. 1998. Inhibition of intraocular neovascularization caused by retinal ischemia in pigs by PKCβ inhibition with LY333531. *Invest. Ophthalmol. Vis. Sci.* **39**:171–179.
19. Koya, D., Haneda, M., Nakagawa, H., et al. 2000. Amelioration of accelerated diabetic mesangial expansion by treatment with a PKCβ inhibitor in diabetic db/db mice, a rodent model of type 2 diabetes. *FASEB J.* **14**:439–447.
20. Nakamura, J., Kato, K., Hamada, Y., et al. 1999. A protein kinase C-β selective inhibitor ameliorates neural dysfunction in stz-diabetic rats. *Diabetes.* **48**:2090–2095.
21. Beckman, J.A., Goldfine, A.B., Gordon, M.B., Garrett, L.A., and Creager, M.A. 2002. Inhibition of PKCβ prevents impaired endothelium-dependent vasodilation caused by hyperglycemia in humans. *Circ. Res.* **90**:5–7.
22. Troller, U., et al. 2001. A PKCβ isoform mediates phorbol ester-induced activation of ERK1/2 and expression of neuronal differentiation genes in neuroblastoma cells. *FEBS Lett.* **508**:126–130.
23. Braiman, L., Sheffi-Friedman, L., Bak, A., Tennenbaum, T., and Sampson, S.R. 1999. Tyrosine phosphorylation of specific protein kinase C isoenzymes participates in insulin stimulation of glucose transport in primary cultures of rat skeletal muscle. *Diabetes.* **48**:1922–1929.
24. Bandyopadhyay, G., Standaert, M.L., Galloway, L., Moscat, J., and Farese, R.V. 1997. Evidence for involvement of protein kinase C (PKC)-zeta and noninvolvement of diacylglycerol-sensitive PKCs in insulin-stimulated glucose transport in L6 myotubes. *Endocrinology.* **138**:4721–4731.
25. Karin, M., Liu, Z., and Zandi, E. 1997. AP-1 function and regulation. *Curr. Opin. Cell Biol.* **9**:240–246.
26. Baeuerle, P.A., and Baltimore, D. 1996. NF-kappa B: ten years after. *Cell.* **87**:13–20.
27. Bogoyevitch, M.A., et al. 1996. Stimulation of the stress-activated mitogen-activated protein kinase subfamilies in perfused heart. P38/RK mitogen-activated protein kinases and c-Jun N-terminal kinases are activated by ischemia/reperfusion. *Circ. Res.* **79**:162–173.
28. Knight, R.J., and Buxton, D.B. 1996. Stimulation of c-Jun kinase and mitogen-activated protein kinase by ischemia and reperfusion in the reperfused rat heart. *Biochem. Biophys. Res. Commun.* **218**:83–88.
29. Yin, T., et al. 1997. Tissue-specific pattern of stress kinase activation in ischemic/reperfused heart and kidney. *J. Biol. Chem.* **272**:19943–19950.
30. Clerk, A., Fuller, S.J., Michael, A., and Sugden, P.H. 1997. Stimulation of "stress-regulated" mitogen-activated protein kinases (stress-activated protein kinases/c-Jun N-terminal kinases and p38-mitogen-activated protein kinases) in perfused rat hearts by oxidative and other stresses. *J. Biol. Chem.* **273**:7228–7234.
31. Laderoute, K.R., and Webster, K.A. 1997. Hypoxia/reoxygenation stimulates Jun kinase activity through redox signaling in cardiac myocytes. *Circ. Res.* **80**:336–344.
32. Hreniuk, D., et al. 2001. Inhibition of c-Jun N-terminal kinase 1, but not c-Jun N-terminal kinase 2, suppresses apoptosis induced by ischemia/reoxygenation in rat cardiac myocytes. *Mol. Pharmacol.* **59**:867–874.
33. Yue, T.-L., et al. 1998. Possible involvement of stress-activated protein kinase signaling pathway and Fas receptor expression in prevention of ischemia/reperfusion-induced cardiomyocyte apoptosis by carvedilol. *Circ. Res.* **82**:166–174.
34. Pombo, C.M., et al. 1994. The stress-activated protein kinases are major c-Jun amino terminal kinases activated by ischemia and reperfusion. *J. Biol. Chem.* **269**:26546–26551.
35. Ozawa, H., et al. 1999. Delayed neuronal cell death in the rat hippocampus is mediated by the mitogen-activated protein kinase signal transduction pathway. *Neurosci. Lett.* **262**:57–60.
36. Chen, L., et al. 2001. Opposing cardioprotective actions and parallel hypertrophic effects of δ PKC and ε PKC. *Proc. Natl. Acad. Sci. U. S. A.* **98**:11114–11119.
37. Dorn, G.W., 2nd, et al. 1999. Sustained in vivo cardiac protection by a rationally designed peptide that causes ε protein kinase C translocation. *Proc. Natl. Acad. Sci. U. S. A.* **96**:12798–12803.
38. Muriel, C.L., and Mochly-Rosen, D. 2003. Opposing roles of δ and ε PKC in cardiac ischemia and reperfusion: targeting the apoptotic machinery. *Arch. Biochem. Biophys.* **420**:246–254.
39. Schulze-Osthoff, K., Ferrari, D., Riehemann, K., and Wesselborg, S. 1997. Regulation of NF-kappa B activation by MAP kinase cascades. *Immunobiology.* **198**:35–49.
40. Karin, M. 1996. The regulation of AP-1 activity by mitogen-activated protein kinases. *Philos. Trans. R. Soc. Lond. B Biol. Sci.* **351**:127–134.
41. Okada, K., et al. 2000. Potentiation of endogenous fibrinolysis and rescue from lung ischemia-reperfusion injury in IL-10-reconstituted IL-10 null mice. *J. Biol. Chem.* **275**:21468–21476.
42. Goldblum, S., Wu, K., and Jay, M. 1985. Lung myeloperoxidase as a measure of pulmonary leukostasis in rabbits. *J. Appl. Physiol.* **59**:1978–1985.
43. Francis, C.W., Marder, V.J., and Martin, S.E. 1980. Plasmic degradation of crosslinked fibrin. I. Structural analysis of the particulate clot and identification of new macromolecular-soluble complexes. *Blood.* **56**:456–464.
44. Lawson, C., et al. 1997. Monocytes and tissue factor promote thrombosis in a murine model of oxygen deprivation. *J. Clin. Invest.* **99**:1729–1738.
45. Goldberg, M., Zhang, H., and Steinberg, S. 1997. Hypoxia alters the subcellular distribution of protein kinase C isoforms in neonatal rat ventricular myocytes. *J. Clin. Invest.* **99**:55–61.
46. Johnson, D., Gautsch, D., Sportsman, J., and Elder, J. 1984. Improved technique utilizing non-fat dry milk for analysis of proteins and nucleic acids transferred to nitrocellulose. *Gene Anal. Tech.* **1**:3–8.
47. Livak, K.J., and Schmittgen, T.D. 2001. Analysis of relative gene expression data using real-time quantitative PCR and the $2^{-\Delta\Delta CT}$ method. *Methods.* **25**:402–408.